Author manuscript, published in "Review of Scientific Instruments 80, 6 (2009) 065102-1/065102-8"
DOI : 10.1063/1.3142486

Quasistatic displacement self-sensing method for cantilevered piezoelectric actuators

Ioan Alexandru Ivan, Micky Rakotondrabe,[a] Philippe Lutz, and Nicolas Chaillet
Department of Automatic Control and Micro-Mechatronic Systems, FEMTO-ST Institute,
UMR CNRS 6174-UFC/ENSMM/UTBM, 24 rue Alain Savary, 25000 Besançon, France

(Received 27 March 2009; accepted 4 May 2009; published online xx xx xxxx)

Piezoelectric meso- and microactuator systems required for manipulation or assembly of microscale objects demand reliable force and/or displacement information. Available sensors are prone to dimension restrictions or precision limitation. Self-sensing method, based on the electric charge measurement, may represent a solution in terms of cost-effectiveness and integration, the actuator performing simultaneously as its own sensor. This paper presents a self-sensing method dedicated to free uni- and bimorph piezocantilevers but can also be adapted to other piezoactuator types. The integrated electric current, used to convert the charge, can be compensated against piezoelectric material nonlinearities to provide accurate displacement information. The advantages relative to existing self-sensing methods consist in the ability to keep this displacement information for long-term periods (more than a thousand seconds) and in the reduction in signal noise. After introductive issues related to the method the base principle allowing the estimation of tip displacement is presented. Then, the identification procedure of the estimator parameters is depicted and representative experimental results are shown. Finally, a series of aspects related to electronic circuits are discussed, useful for successful system implementation.

I. INTRODUCTION

Piezoelectric cantilevered actuators usually made up of one or two piezoelectric layers (called uni- or bimorph) are present in many micromanipulation and microrobotic applications, thanks to their high displacement resolution and fast response time. The static and dynamic behaviors of piezoelectric actuators, their inherent nonlinearities (hysteresis and creep), and limits were studied and modeled[1–4] especially during the past 2 decades in attempting to provide more efficient control solutions.[5–7]

In order to perform very accurate and fast response time closed-loop micromanipulation tasks, various sensors have been used. Unfortunately, these sensors are not ideally adapted to the micro- and nanoworld because of their sizes, performances, and limited measurement of degrees of freedom. Table I summarizes mostly available sensors in the field. Hence, an alternative to the use of sensors is the self-sensing method. There are several advantages of the self-sensing method relative to the use of external sensors. Among them, it allows a consistent reduction in the costs by eliminating expensive sensors. As can be seen, resolution can also be submicrometric and comparable to that of external sensors. Self-sensing is based on charge conversion. In fact, charge is nearly proportional to the displacement, hence there is no need to further compensate the complex nonlinearities (hysteresis and creep) such as in (Ref. 8).

The idea of self-sensing in piezoelectric cantilever has been started by the work of Dosch *et al.*[9] While it is not a new concept on vibration damping or control,[10–13] more recently, it has shown its feasibility for piezoelectric tubes of atomic force microscopy.[14,15] But to our knowledge, self-sensing methods have not yet been adapted for long-term (more than hundreds of seconds) displacement measurement of cantilevered actuators, as required by micromanipulation and microrobotic tasks. In this paper, we present a compensated self-sensing approach especially dedicated to long-term static measurement. We especially focus on the displacement measurement of a piezoelectric cantilever beam.

Drawbacks of displacement self-sensing method refer to inherent charge leaks and temperature influence. With proper actuators and electronic circuits, charge information may be preserved even for thousands of seconds. However, because of the temperature variations, extra care will be required for proper thermal isolation especially in the case of nonsymmetric cantilevers (example: unimorph) to limit temperature-related uncertainties.

There are several self-sensing schematics depending on application. Capacitive bridges[9,11] are convenient for vibration control but are not easy to balance for long-term measurements. Structures with both electrodes for actuation and electrodes for sensing are a simple solution but their inconvenience is a partial reduction in the total actuating range.[14,16] A current integrator was introduced in Ref. 17 for a piezostack. The disadvantage was a poor compensation of leaking resistance with a very high value potentiometer across the integrating capacitor. Another method quite related to self-sensing concept was linearization of the actuator displacement using voltage-to-charge amplifiers.[18,19] The ad-

---

[a] Author to whom correspondence should be addressed. Electronic mail: mrakoton@femto-st.fr.

TABLE I. Displacement sensors for the microworld.

Sensor type	Advantages	Disadvantages
Triangulation lasers	High precision and resolution; fair band pass; and spot measurement	Quite expensive, large sizes, and limited measurement range
Interferometers	Very high precision resolution and range; increased band pass; and spot(s) measurement	Very expensive and large sizes
Diffraction grating target	High precision and multidimensional measurement	Large sizes, require attaching target, and expensive
Strain gages	Less expensive and millimeter size	Fragile, noisy output signal, and temperature influence
Capacitive or inductive	High sensibility, high precision, and fair price	Require linearization, from fair to quite large dimensions, and close vicinity requirements
Magnetic Hall effect, magnetoresistive, and magnetostrictive	Good precision, band pass, and fair price	Require permanent magnets often too large and close vicinity requirements.
Using image processing	Large measurement range and in-plane displacement	Expensive and limited resolution and response time
Piezoelectric self-sensing	Double functionality, high band pass, high resolution, and lowest price	Require nonlinear compensation and long-term charge leaking

vantage was a linear voltage-to-displacement characteristic. However, the conventional HV supplier needs to be replaced by more complex charge driven circuits. In our paper we propose two simple schematics of current integrators (modified charge amplifiers) that can also be easily implemented onto existing systems, avoiding requiring the redesign of actuator or HV supply.

The developed self-sensing systems can be divided into three main parts, as in Fig. 1: the piezoelectric actuator, the electronic circuit, and the data processing system. The latter is the proposed self-sensing estimator. The estimate displacement could be used for further feedback or closed-loop control systems.

Piezoelectric actuators are submitted to V_{in} external voltages in a range of up to several hundred volts, depending on actuators. Resulted charge Q (in fact integrated current) is converted by the electronic amplifier to a measurable voltage V_{out}. This signal will be converted for further numerical processing. Data is further processed on a computer or is deployed into a real-time processor or microcontroller. External signals can be provided to improve the self-sensing accuracy, for instance temperature variation may be compensated with a small thermistor. As the charge cannot be kept indefinitely, external resetting before each measurement prevents saturation and offsets large parts of the static error.

Among the contributions of this paper include: the introduction of an antiparallel reference capacitance, numerical compensations of amplifier bias currents and of piezoelectric leaking resistance, and dielectric absorption. A step by step approach of the identification of the self-sensing parameters is presented as well as experimental results.

The paper is organized as follows. First, we present the principle and related equations of the self-sensing estimator. Afterwards, we detail the parameter identification. Hence, we present the experimental results. Finally, we relate some issues to be taken into account when deploying self-sensing systems.

II. DISPLACEMENT DETECTION

A. Charge output of piezoelectric cantilever

Consider a bimorph cantilevered beam piezoactuator subjected to an electrical excitation V_{in} (Fig. 2). The beam is characterized by its length L, its width w, and its half-thickness h.

In the absence of external force, we have a theoretically linear relation between displacement and applied voltage[20]

$$\delta = -\frac{3d_{31}}{1+\frac{d_{31}^2}{4s_{11}^E\varepsilon_{33}^S}}\frac{L^2}{h^2}V_{\mathrm{in}}, \tag{1}$$

where s_{11}^E is the compliance coefficient along the beam (X direction), ε_{33}^S and d_{31} are dielectric and piezoelectric material coefficients.

Using the relation between the applied voltage and the capacitance for bimorph piezoelectric cantilever beam

$$Q = \frac{4wL\varepsilon_{33}^S}{h}V_{\mathrm{in}}, \tag{2}$$

charge directly results and, as stated previously, is quasiproportional to free displacement δ

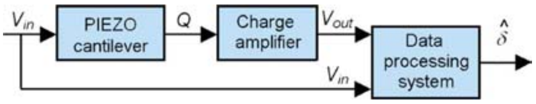

FIG. 1. (Color online) Displacement self-sensing system.

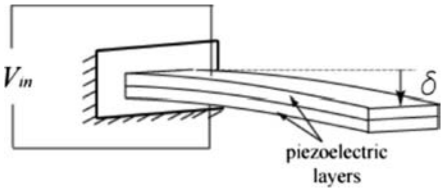

FIG. 2. A bimorph piezoelectric cantilever beam.

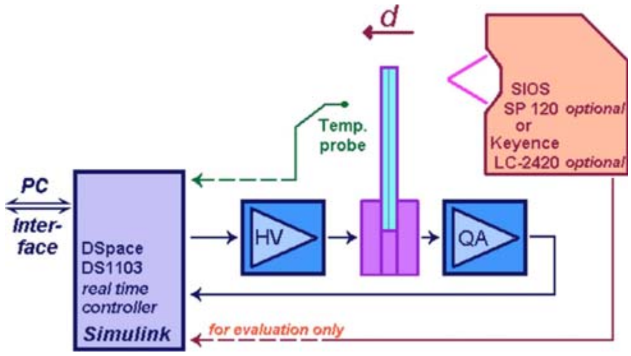

FIG. 3. (Color online) Experimental setup schematic of the self-sensing actuator. Direction for positive displacement is given.

$$Q = \frac{4wh\varepsilon_{33}^{S}}{3d_{31}L}\left(1 + \frac{d_{31}^{2}}{4s_{11}^{E}\varepsilon_{33}^{S}}\right)\delta = \alpha\delta, \tag{3}$$

where α is denoted as an actuator charge-displacement coefficient. In the sequel, this charge will be converted into a measurable voltage V_{out} from which the deflection δ will be estimated, as described in Fig. 1.

B. Experimental setup

A schematic overview of the setup is depicted in Fig. 3. Several uni- and bimorph rectangular actuators (PZT on Cu or Ni substrate) were tested, of length between 10–15 mm, width between 1–2 mm, and total thickness of 0.27–0.45 mm. A Keyence LC-2420 optical displacement reader was only used for intermediate tests on actuators displacement; for some measurements requiring better precision a SIOS SP-120 miniature plane-mirror interferometer was employed (Fig. 4). However displacement readings served only for referencing and evaluating purposes of the self-sensing method. The high voltage (HV) amplifier allowed applying a voltage up to ±150 V. A current integrator amplifier circuit (modified charge amplifier) to be discussed next chapter provided V_{out} output signal. The Matlab Simulink detection model was deployed on a high speed DSpace DS1103 real-time controller board. A PC-based CONTROLDESK interface served for model parameterization and data acquisition/presentation.

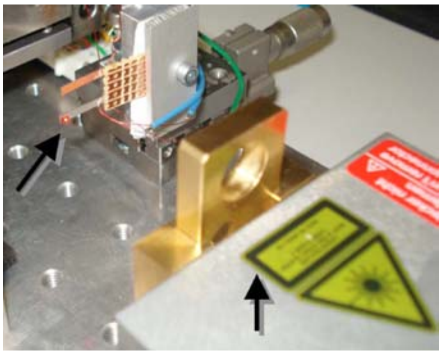

FIG. 4. (Color online) Photo of experimental setup. Actuator is placed in the upper left and SIOS interferometer is in the right side of the image.

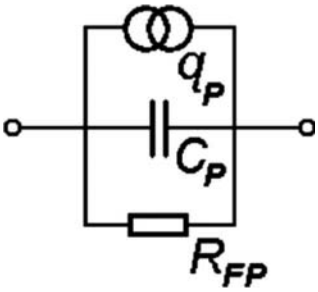

FIG. 5. Equivalent electrical schematic of a piezoactuator.

C. Integrator amplifier

The static electrical equivalent schematic of piezoelectric bender is a charge generator in parallel with a capacitor and a leaking resistance, as seen in Fig. 5, and its electromechanical model is shown in Ref. 2. C_P capacitance is in the order of nanofarad depending on the shape and dimensions of the microactuator's structure while R_{FP} is the insulating resistance, whose order of magnitude is between $10^{9}\ldots10^{12}\ \Omega$.

If we ignore nonlinear effects, charge is proportional to the applied voltage and the external force. To measure charge, we propose a precise integrator circuit scheme, as pictured in Fig. 6 and described below.

The input signal V_{in} is inverted and applied to a "reference capacitor" C_R whose the value is close to C_P value; it will "absorb" a significant part of the charge due to the applied voltage, according to the second Kirchoff law. Although C_R and HV inverter may miss from the circuit, their use is recommended. Indeed, the output will saturate at a higher V_{in} input voltage value (up to several hundred volts) while preserving the same sensitivity. Feedback capacitor C will integrate the current due to external force variation and applied voltage (depending on C_R/C_P fraction). An electromechanical relay-switch k (in series with several kilo ohms resistor) allows resetting V_{out} voltage from DSpace environment in order to avoid the saturation. Electronic switches are not suitable because of their "off" source/drain leakage currents. Further details and propositions are discussed in Sec. V.

Output voltage is

$$V_{\text{out}} = -\frac{1}{C}\int_{0}^{T} i(t)dt = -\frac{1}{C}Q, \tag{4}$$

where, for the free beam (F_{ext}=0), charge is

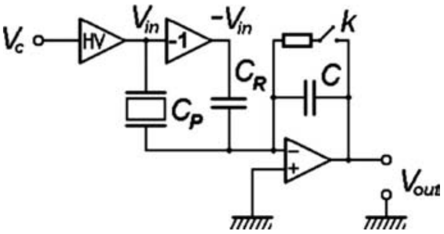

FIG. 6. Electronic circuit schematic of charge amplifier.

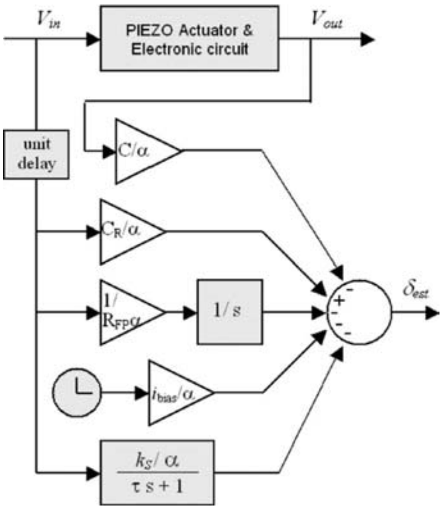

FIG. 7. Displacement detection model (Simulink).

$$Q = -C_R V_{\text{in}} + \alpha\delta, \tag{5}$$

where α was introduced in Eq. (3).

If we consider a nonlinear dielectric absorption effect of piezoelectric material, we propose the following slight modification:

$$Q = -C_R V_{\text{in}} + (\alpha\delta + Q_{\text{DA}}), \tag{6}$$

where Q_{DA} is an internal amount of charge depending on ε_{33} variation.

D. Detected displacement formula

Adding the influence of the nonzero bias current i_{BIAS} of the operational amplifier (op-amp) and finite leaking resistance R_{FP} of the piezoactuator, output voltage V_{out} of the free cantilever beam is given by

$$V_{\text{out}} = \frac{C_R}{C}V_{\text{in}} - \frac{\alpha\delta + Q_{\text{DA}}}{C} - \frac{1}{C}\int \frac{V_{\text{in}}(t)}{R_{\text{FP}}}dt - \frac{1}{C}\int i_{\text{BIAS}}(t)dt. \tag{7}$$

Extracting the displacement δ, we obtain the estimate as follows:

$$\delta_{\text{est}} = -\frac{C}{\alpha}V_{\text{out}} - \frac{Q_{\text{DA}}(V_{\text{in}},t)}{\alpha} + \frac{C_R}{\alpha}V_{\text{in}} - -\frac{1}{R_{\text{FP}}\alpha}\int V_{\text{in}}(t)dt - \frac{1}{\alpha}\int i_{\text{BIAS}}(t)dt. \tag{8}$$

We will consider a simple relaxation effect described by a first-order transfer function for the dielectric absorption term

$$Q^*_{\text{DA}}(s) = \frac{Q_{\text{DA}}(s)}{\alpha} = \frac{k^*_s}{\tau s + 1}, \tag{9}$$

where static gain $k^*_s = k_s/\alpha$. Based on the previous equations, Fig. 7 presents the detailed estimation bloc-scheme. Some parameters of the identification in Eq. (8) have to be identified. It will be presented in the next section.

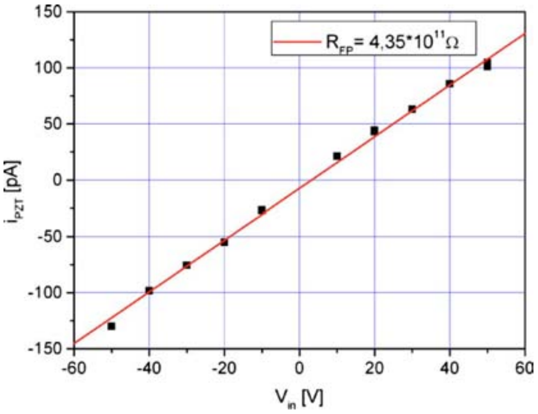

FIG. 8. (Color online) Leakage current of PZT actuator measured under constant dc voltage values. Calculated insulation resistance is 0.435 TΩ.

III. SELF-SENSING PARAMETER IDENTIFICATION

Parameters identification of Eq. (8) can be performed under a manual or semiautomatic procedure. Capacitances are given (C=47 nF and C_R=8.2 nF in our case). The identification procedure for the rest of parameters (α, i_{BIAS}, R_{FP}, and Q_{DA}) is based on Eq. (7), where the displacement δ is provided by the displacement sensor (optical or interferometer). The following steps describe the identification procedure.

A. Bias current i_{BIAS} identification

Under F_{ext}=0, V_{in}=0, $V_{\text{out}}\cong 0$, and zero temperature change, there is no electric current through the piezoelectric material; the V_{out} rate of change is measured for several dozens of seconds, deriving i_{BIAS}.

B. Leaking resistance R_{FP} identification

Under F_{ext}=0, a constant voltage $V_{\text{in}} \neq 0$ is applied to the actuator. After several hundred seconds the creep influence becomes negligible, and the output voltage V_{out} shifts with a constant slope, depending on i_{BIAS} (identified before) and R_{FP} (to be identified).

The identification can be repeated for different V_{in} values and averaged. Each point in Fig. 8 was recorded after a 1000–2000 s delay, to eliminate residual creep influence. Linear regression was applied.

Quality piezocantilevers will exhibit R_{FP} values superior to 1010 Ω. For our actuator we identified R_{FP}=0.435 TΩ.

C. Displacement coefficient α identification

A step signal is applied on the free actuator. To avoid dynamic oscillations of the actuator, the step signal is shaped with ramp of around 20 V/s (Fig. 9). Measured values of δ and V_{out} immediately after V_{in} step signal will serve to compute α

$$\alpha = (-CV_{\text{out}} + C_R V_{\text{in}})/\delta. \tag{10}$$

An alternate method for deriving α is to apply one or several sinusoidal signals as in Fig. 10 and use amplitude values in Eq. (10).

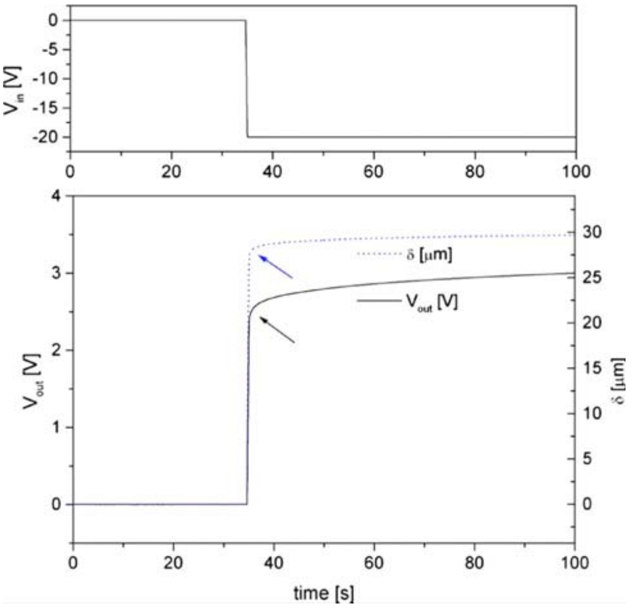

FIG. 9. (Color online) Identification of α coefficient with a -20 V ramped step input.

D. Identification of dielectric absorption transfer function

The last part to be identified in displacement in Eq. (8) is the dielectric absorption $Q_{\mathrm{DA}}(V_{\mathrm{in}},t)$ of the piezoelectric material.

$$\Delta\delta_{\mathrm{est}}(s) = Q^{*}_{\mathrm{DA}}(s)V_{\mathrm{in}}(s), \tag{11}$$

where $\Delta\delta_{\mathrm{est}}=\delta_{\mathrm{est}}-\delta$ is the difference between estimated (using already identified parameters) and measured tip displacements (Fig. 11). Identification of k_s and τ is performed on a step response, calculating the static gain and response time to reach 63.2% of final value.

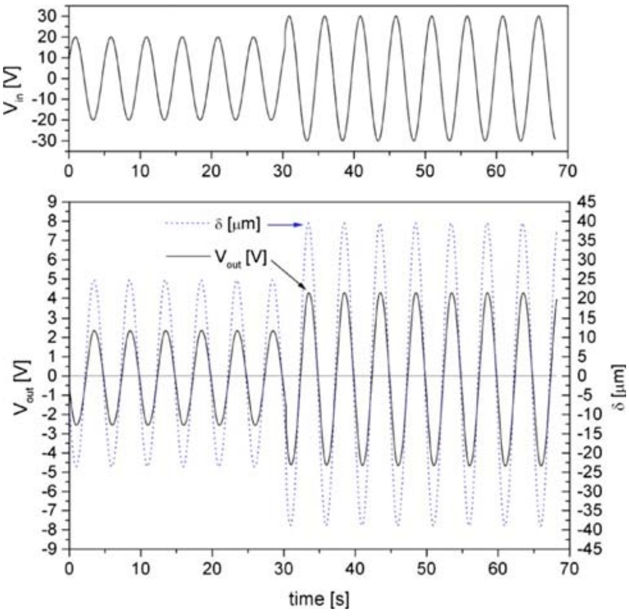

FIG. 10. (Color online) Identification of α coefficient from sinusoidal signals.

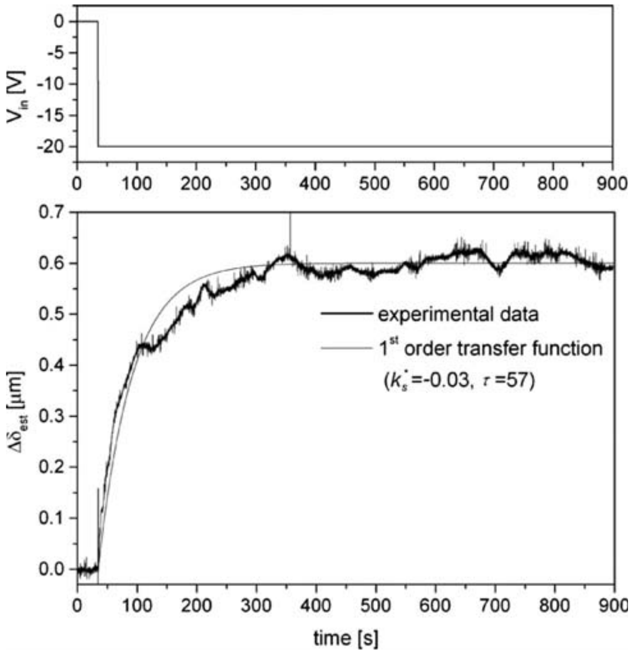

FIG. 11. Identification of dielectric absorption $Q^{*}_{\mathrm{DA}}(s)$ transfer function.

IV. SELF-SENSING RESULTS

Several tests have been performed to evaluate the accuracy of the proposed self-sensing technique. Known and identified parameters are entered into the real-time processor, we have

$$\alpha = -10.05e^{-9}\ \mathrm{C/m},$$

$$C = 47e^{-9}\ \mathrm{F},$$

$$C_P = 1.74e^{-9}\ \mathrm{F},$$

$$C_R = 8.2e^{-9}\ \mathrm{F},$$

$$R_{\mathrm{FP}} = 0.435e^{12}\ \Omega,$$

$$i_{\mathrm{BIAS}} = -1.7e^{-12}\ \mathrm{A},$$

$$\tau = 57\ \mathrm{s},$$

$$k_s = 3.02e^{8}\ \mathrm{m/V}.$$

A. Displacement self-sensing results

In Fig. 12, an input signal V_{in} was applied in several steps between +20 and -25 V, under null external force. Data was recorded for 1020 s—largely sufficient for most applications involving piezoelectric actuators. A very good agreement is found; measured and detected displacement curves almost superpose.

A comparative representation of displacement errors is made as follows. Three graphs are traced (Figs. 13–15) from uncompensated to fully compensated with respect to leaking resistance and dielectric absorption. Measurement with Keyence optical displacement reader provided a poorer linearity than self-sensing signal, making it impossible for accurate error evaluation; SIOS interferometer was eventually em-

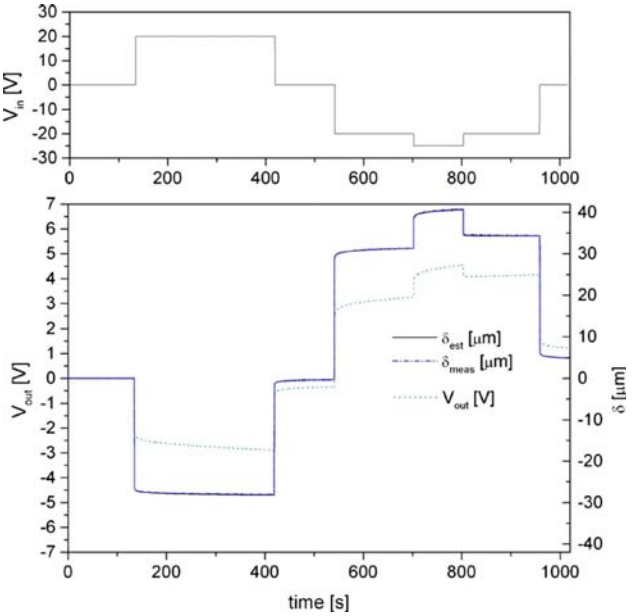

FIG. 12. (Color online) Measured and detected displacement for an arbitrary V_{in} input signal ($F_{ext}=0$).

ployed. Our constraint on the utilized interferometer is that data is only available offline. Vertical error lines in the figures can be neglected and are due to the linear interpolation and sampling period mismatch between the two data sets (acquired at sampling rates of 10 and 16.11 Hz).

As seen in the Fig. 13, peak-to-peak error of uncompensated signal is 2.75 µm. Compensation of R_{FP} leaking resistance allowed a reduction in maximum error to 1.05 µm (Fig. 14). Adding the compensation of dielectric absorption (Fig. 15) provided a 0.38 µm (0.55%) peak-to-peak error.

Unaveraged measured self-sensing signal noise in displacement is of only 1.6 nm (rms), being 10 times less noisy than that of filtered Keyence LC-2420 sensor (16.7 nm rms noise on 4096 averaged samples). However, as expected, SIOS SP 120 interferometer showed best results: 0.5 nm rms noise (Fig. 16).

B. Temperature influence on displacement self-sensing accuracy

Temperature exhibits changes in dielectric and piezoelectric constants. Also, differences in thermal expansion of piezoelectric and passive material tend to bend the structure like a thermal bimetallic, conducting to parasitic displacement (and charges). In this case Eq. (2) between charge and displacement no longer applies ($Q \neq \alpha\delta$), leading to displacement errors. To analyze the thermal influence, we compared its effects on two types of piezoelectric beams: unimorph and bimorph cantilevers. As seen in figures and as expected, unimorphs (Fig. 17) are more affected by ambient temperature than bimorphs (Fig. 18). As bimorph cantilevers are intrinsically symmetric, charges from both sides sum up and self-compensate.

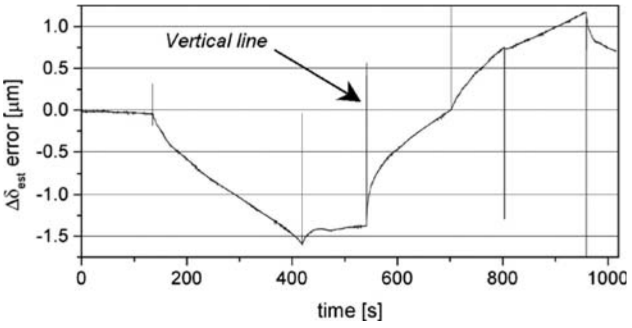

FIG. 13. Error curve of detected displacement with no leaking resistance R_{FP} and dielectric absorption Q_{DA} compensation.

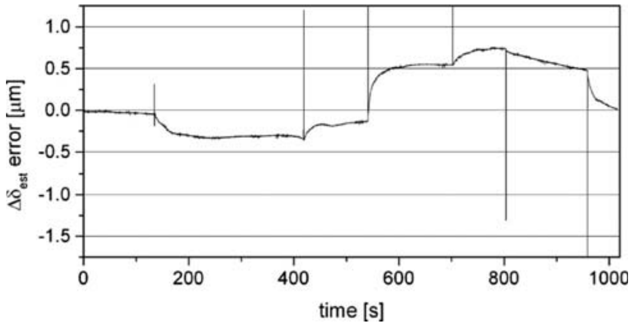

FIG. 14. Error curve of detected displacement with only leaking resistance R_{FP} compensation.

If we compare the above results, we see that unimorph cantilevers are five times more sensitive to temperature than bimorphs. Errors can be limited by a proper thermal isolation or compensated with a sensitive temperature sensor like a miniature thermistor. However, temperature sensor should be in contact with the actuator for more correlate readings.

V. CURRENT INTEGRATION RELATED ISSUES

An improper choice of charge amplifier[21] will significantly reduce sensing accuracy. The circuit should be protected against temperature changes, with a special care to PCB design (guard rings, sufficient space between routes, vias, and pads) otherwise unwanted leakage will easily exceed op-amp bias current.

Integrating capacitor must have primarily an extremely high insulation resistance, low dissipation factor, and good temperature stability. Polypropylene plastic film capacitors were employed in our case, with a measured leaking resistance of 24 TΩ for $C=10$ nF, high enough to ignore its

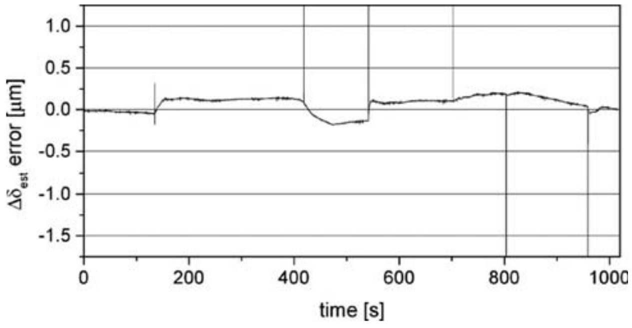

FIG. 15. Error curve of detected displacement with compensation of leaking resistance R_{FP} and dielectric absorption Q_{DA}.

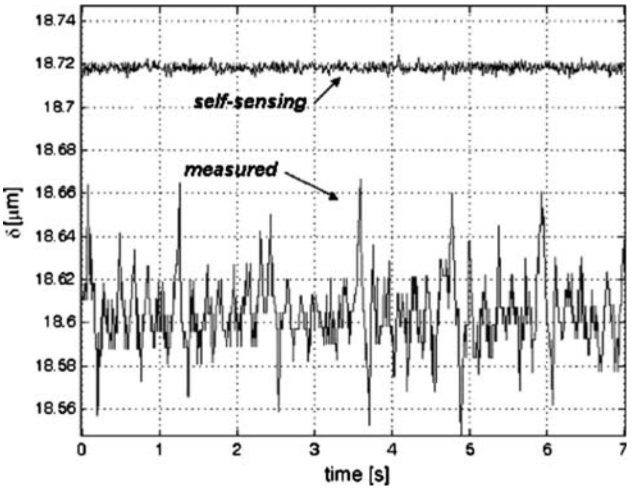

FIG. 16. Zoomed in measure (Keyence LC2420) and detected displacement for noise evaluation.

leaking influence in the circuit. Polystyrene or Teflon capacitors also showed better performance than ceramic or polyester film capacitors.

Precise operational amplifiers used in charge amplifiers must be unity-gain stable; otherwise they will tend to oscillate. Noise and bias currents have to be as small as possible. Several op-amp types were tested, OPA111BM Difet model was chosen for its very small bias current (1.7 pA), small offset voltage, small temperature drift, fair supply voltage, and on-chip guarding ring. OPA627 model is also suitable.

Attention has must be paid to supply and input voltages. The circuit is damaged if high input voltage is applied in the absence of supply voltage. Also, to prevent the output saturation, the *k* switch allows resetting when necessary. Further increase in voltage over an already saturated op-amp will cause damage.

Cables should be shielded properly to avoid the electromagnetic interference. Further noise rejection can be achieved by modifying the electronic schematic presented in Fig. 6. We propose the schematic pictured in Fig. 19 where the current, proportional to the voltage drop across a series resistance or more likely across a voltage divider (to avoid op-amp damage due to HV), is buffered or preamplified and then integrated. Indeed, this schematic allows noise reduction thanks to the grounded series resistance R_{Z_2} connected to the high impedance amplifier input.

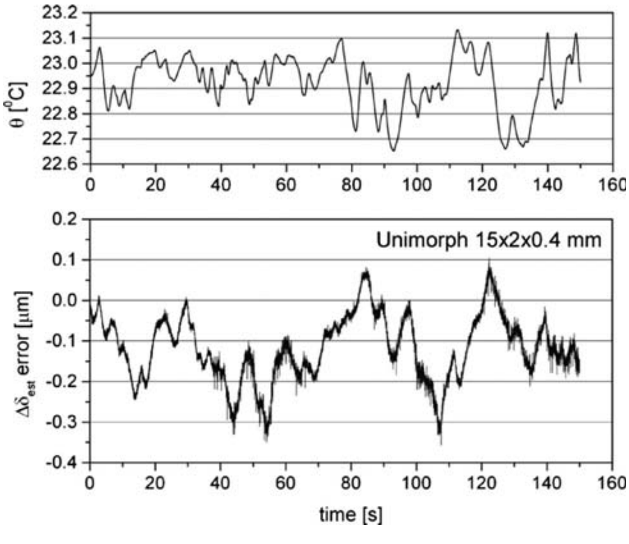

FIG. 17. Typical self-sensing displacement error due to ambient temperature change in a unimorph actuator. Error is ~1 μm/°C.

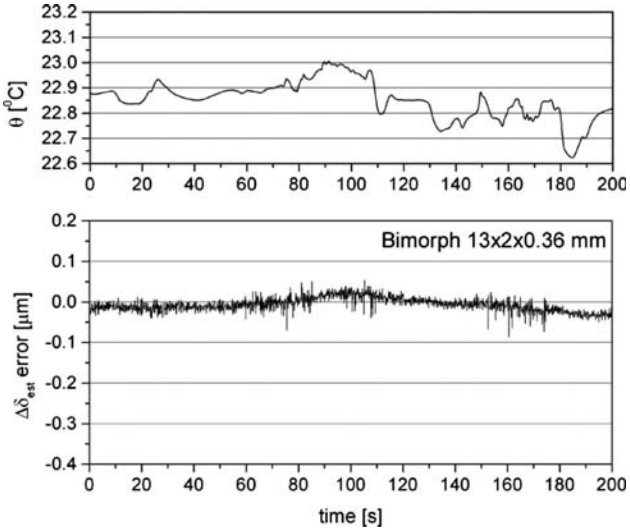

FIG. 18. Typical self-sensing displacement error due to ambient temperature change in a bimorph actuator. Error is ~0.2 μm/°C.

$$V_{\text{out}} = -\frac{R_{Z_2}}{RC(R_{Z_1}+R_{Z_2})}\int_0^T i(t)dt, \tag{12}$$

For our actuator the best compromise between response time, sensitivity, and noise was a series resistance of 82 kΩ ($R_{Z_1} + R_{Z_2} = 82$ kΩ).

Noise was reduced by a factor of five but on the other hand this schematic was much more sensitive to temperature offset drifts than that of Fig. 6. As V_z voltage is in the μV range or lower, op-amp offset voltage temperature drift (±0.5 μV/°C) and supply rejection (±3 μV/V) limited system accuracy. Usually op-amp offset is trimmed manually (with potentiometers); in our case this measure was not sufficient to compensate thermal drifts. We made an automatic compensation of the offset voltage with random temperature changes. This was performed by connecting DSpace DAC outputs (Fig. 20) to op-amp "trim" pins and by measuring and referencing the temperature to a miniature thermistor in close contact with op-amp chip. This way, we preserved a signal up to 100 s similar in accuracy with that of Figs. 12–15, however rms noise was reduced from 1.6 nm to only 0.4 nm, inferior to even that of SIOS SP120 interferometer.

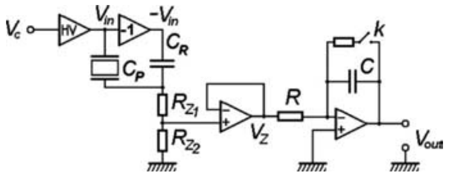

FIG. 19. Alternate schematic with voltage divider and integrator allowed noise reduction.

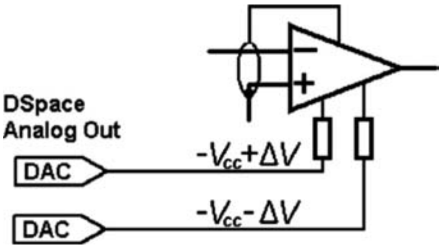

FIG. 20. Offset drift compensation connecting DSpace output to trim pins.

Zero-drift chopper op-amps (typically $\pm 0.03\ \mu V/^{\circ}C$) will probably ameliorate temperature drifts but other effects such as thermal electro motive force (EMF) (Seebeck effect) in cable junctions will still perturbate the circuit.

To generally resume, charge integration is prone to nonzero bias currents offset voltages, temperature drifts, leaking resistance or currents, thermal EMF and electro magnetic interference influence. However, with proper measures, their influence can be eliminated or at least partially quantified and compensated.

VI. CONCLUSION

Displacement self-sensing of uni- and bimorph cantilevered actuators used for meso- and microscale gripping and manipulation is cost-effective and relatively simple to implement or upgrade to existing systems. To our knowledge it is a first paper focusing on displacement self-sensing of these devices. We referred to a current integration method self-compensated against some actuator nonlinearities (hysteresis and creep) and externally compensated to others (leaking resistivity and dielectric absorption).

In the case of detected or *a priori*—supposed absence of external forces, displacement is almost directly proportional to the charge. Further compensation of nonzero amplifier bias current, finite actuator leaking resistance, and dielectric absorption lead to a significant reduction in errors, up to 0.55% and an increase in measurement period to more than 1000 s, sufficient enough for most tasks. Signal noise was lower than that measured with expensive laser triangulation sensor. Two schematics were presented, the first one based on direct current integration showed its feasibility for long integration periods while the second integrating shunt voltage drop allowed a further reduction in signal noise with a cost of a more unstable long-term signal. Practical issues related to long-term charge preservation were presented, and temperature influence discussed.

ACKNOWLEDGMENTS

The authors especially thank Roger Bourquin, professor at ENSMM Besancon, France, for helpful discussions. This work is supported by the EU FP7 SP3-People Program under Grant No. PIEF-GA-2008–219412 (New Micro-Robotic Systems featuring Piezoelectric Adaptive MicroStructures for Sensing and Actuating, with Associated Embedded Control).

[1] T. S. Low and W. Guo, J. Microelectromech. Syst. **4**, 230 (1995).
[2] H. J. M. T. A. Adriaens, W. L. de Koning, and R. Banning, IEEE/ASME Trans. Mechatron. **5**, 31 (2008).
[3] Y.-G. Zhou, Y.-M. Chen, H.-J. Ding, and W.-Q. Chen, J. Zhejiang Univ. Sci. A. **9**, 1 (2008).
[4] R. J. Wood, E. Steltz, and R. S. Fearing, Proceedings of the IEEE International Conference on Robotics and Automation, Spain, 2005 (unpublished).
[5] H. Jung and D.-G. Gweon, Rev. Sci. Instrum. **71**, 1896 (2000).
[6] M. Rakotondrabe, C. Clévy, and P. Lutz, IEEE Trans. Autom. Sci. Eng. (unpublished).
[7] M. Rakotondrabe, Y. Haddab, and P. Lutz, IEEE Trans. Control Syst. Technol. **17**, 528 (2009).
[8] M. Rakotondrabe, Y. Haddab, and P. Lutz, Proceedings of the IEEE/ASME International Conference on Advanced Intelligent Mechatronics, Zurich, Switzerland, September 2007 (unpublished), pp. 1–6.
[9] J. J. Dosch, D. J. Inman, and E. Garcia, J. Intell. Mater. Syst. Struct. **3**, 166 (1992).
[10] W. W. Law, W.-H. Liao, and J. Huang, Smart Mater. Struct. **12**, 720 (2003).
[11] P. C. Khiang, G. Guoxiao, M. B. Chen, and T. H. Lee, IEEE/ASME Trans. Mechatron. **11**, 328 (2006).
[12] G. A. Lesieutre, Shock Vib. Dig. **30**, 187 (1998).
[13] S. O. R. Moheimani, IEEE Trans. Control Syst. Technol. **11**, 482 (2003).
[14] S. O. R. Moheimani and Y. K. Yong, Rev. Sci. Instrum. **79**, 073702 (2008).
[15] S. O. R. Moheimani, Rev. Sci. Instrum. **79**, 071101 (2008).
[16] D. Campolo, R. Sahai, and R. S. Fearing, Proceedings of the IEEE International Conference on Robotics and Automation, Taipei, 2003 (unpublished), Vol. 3, pp. 3339–3346.
[17] Y. Cui, Proceeding of the Sixth World Conference on Intelligent Control and Automation, China, 2006 (unpublished).
[18] J. Agnus and N. Chaillet, INPI Patent No. FR 03000532 (August 2004).
[19] A. J. Fleming and S. O. R. Moheimani, Rev. Sci. Instrum. **76**, 073707 (2005).
[20] J. G. Smits and W.-S. Choi, IEEE Trans. Ultrason. Ferroelectr. Freq. Control **38**, 256 (1991).
[21] J. Karki, Texas Instr. Appl. Report No. SLOA033A, 2000.